



Estimating iron and aluminum removal rates in the eastern equatorial Pacific Ocean using a box model approach

Artur P. Palacz^{a,*}, Fei Chai^a, Richard C. Dugdale^b, Christopher I. Measures^c

^a School of Marine Sciences, University of Maine, Orono, ME 04469, USA

^b Romberg Tiburon Center, San Francisco State University, 3152 Paradise Drive, Tiburon, CA 94920, USA

^c Department of Oceanography, University of Hawai'i at Manoa, Honolulu, HI 96822, USA

ARTICLE INFO

Article history:

Received 9 August 2010

Accepted 9 August 2010

Available online 19 August 2010

Keywords:

Fe transport and cycling

Al scavenging

Box model

HNLC waters

Geographic region: equatorial Pacific

ABSTRACT

Iron limitation plays an important role in maintaining the high-nitrate low-chlorophyll (HNLC) condition in the equatorial upwelling zone. The rate and depth of upwelling control Fe supply to the euphotic zone. This study constrains the transport fluxes and budget of two trace metals, Fe and Al, in the upper ocean. They are co-delivered to the eastern equatorial Pacific surface waters via the Equatorial Undercurrent and upwelling but show distinct biogeochemical cycling processes.

We combine the results of the *in situ* measurements of dissolved Fe and Al (dFe and dAl) with the modeled velocity fields to calculate the physical fluxes. The model calculations are evaluated with the conservation of heat, volume transport, NO₃ and Si(OH)₄ budgets for the equatorial Pacific. The vertical flux due to upwelling provides averaged dFe and dAl supply rates of 1.45 μmol m⁻² d⁻¹ and 11.51 μmol m⁻² d⁻¹, respectively. The sum of the net physical fluxes in the eastern equatorial Pacific for dFe and dAl are 0.41 μmol m⁻² d⁻¹ and 2.77 μmol m⁻² d⁻¹, respectively. These estimates are equal to the net biological and chemical removal rates of dFe and dAl. The calculated dFe:C net removal ratio is in the range of 3–9 μmol:mol, which agrees with most other estimates. This suggests that the majority of net dFe removal is due to biological uptake in the upper water column.

The results of this box model approach illustrate the usefulness of combining the modeled outputs and *in situ* measurements, which provide additional constraints on Fe transport and cycling in the equatorial Pacific and possibly other HNLC regions.

© 2010 Elsevier Ltd. All rights reserved.

1. Introduction

The equatorial Pacific has become a subject of extensive field, laboratory and modeling studies during the last couple of decades in part due to two important characteristics and their link to the global carbon cycle. Firstly, a vast part of the eastern equatorial Pacific Ocean is considered as high-nitrate low-chlorophyll (HNLC) region (Barber and Chavez, 1991; Murray et al., 1994) and by Dugdale and Wilkerson (1998) as a high NO₃, low Si(OH)₄, low chlorophyll (HNLSiC) waters; yet, it accounts for almost 10% of the global ocean productivity (Pennington et al., 2006). Secondly, the equatorial upwelling zone is the largest source of CO₂ flux from the ocean to the atmosphere, at about 0.7–1.0 × 10¹⁵ gC y⁻¹ (Feely et al., 1999; Takahashi et al., 2003; Pennington et al., 2006). Observational and modeling studies have proposed that atmospheric CO₂ concentrations are partially regulated by nutrient and dissolved inorganic carbon (DIC) removal by phytoplankton during photosynthesis (Martin et al.,

1990; Sarmiento and Orr, 1991), hence the interest in processes regulating the phytoplankton growth in the eastern equatorial Pacific (EEP). Martin et al. (1990) hypothesized that the supply of Fe must play an important role in controlling the primary production in this region. Several experiments carried out in this region (Martin and Fitzwater, 1988; Martin et al., 1991, 1994; Coale, 1991; Greene et al., 1994) have confirmed that low Fe concentrations are a physiological constraint on phytoplankton growth, especially for diatoms. Limited available concentration of Si(OH)₄ can also interact with the rate of diatom growth (Dugdale and Wilkerson, 1998; Dugdale et al., 2002a, 2007). The diatoms are responsible for up to 60% of NO₃ uptake in the EEP (Dugdale et al., 2007), thus low Si(OH)₄ also affects primary productivity in the equatorial Pacific. Based on growout experiments Brzezinski et al. (2008) reported that Si and Fe together controlled diatom uptake rates of Si(OH)₄ by almost a factor of 3, which suggests co-limitation by Fe and Si. However, no relationship between ambient Fe concentrations and Si(OH)₄ or NO₃ uptake could be found in the study area during the 2004 and 2005 Equatorial Biocomplexity (EB04 and EB05) cruises. The question of the relative dominance of Fe and Si limitation is discussed in several other manuscripts in this issue (Baines et al., 2011; Balch

* Corresponding author. Tel.: +1 207 581 4338.

E-mail address: artur.palacz@umit.maine.edu (A.P. Palacz).

et al., 2011; Brzezinski et al., 2011; Demarest et al., 2011; Dugdale et al., 2011). Zooplankton grazing exerts strong pressure on the phytoplankton community and might additionally keep the total phytoplankton biomass below the level that could be supported by available nutrients (Cullen et al., 1992). It is likely that it is the combination of several factors that result in the persistent HNLC conditions in the EEP (Chavez et al., 1991; Frost, 1991; Price et al., 1991; Chai et al., 1996; Landry et al., 1997).

Fe supply is said to regulate a wide range of marine biogeochemical processes (Morel and Price, 2003). It affects the autotrophic community through algal physiology (Boyd, 2002) and phytoplankton species composition (Bruland et al., 2001), but also impacts the heterotrophic community through physiological aspects of microzooplankton (Chase and Price, 1997) and heterotrophic bacteria (Tortell et al., 1996). Nonetheless, our knowledge of the biogeochemical cycling of Fe remains insufficient to understand its role in regulating the biological productivity in the EEP. Fe chemistry in sea water is controlled both by complex inorganic and biologically mediated processes. In the open ocean, organic complexation mostly via biological uptake and particle scavenging maintains total dissolved Fe levels above those predicted by the solubility of the inorganic species (Rue and Bruland, 1995; Rue et al., 1997; Macrellis et al., 2001; Wu et al., 2001). Depending on the source of Fe, its solubility as well as bioavailability will differ considerably.

Although Johnson et al. (1997) concluded that high coastal Fe concentrations do not normally penetrate far into the open ocean, the Equatorial Undercurrent (EUC) is now believed to be the main source of Fe and Al to the EEP surface waters (Wells et al., 1999; Christian et al., 2002; Slemons et al., 2009; Gorgues et al., 2010). The EUC is an eastward flowing subsurface current, with a core depth of about 200 m that shoals upward from west to east, stretching over some 13,000 km along the equator (Stewart, 2007). While atmospheric deposition is considered to be the main source of Fe to surface waters globally (Duce and Tindale, 1991), it is the upwelling of nutrient-enriched EUC waters that controls the supply of dissolved Fe (dFe) to the euphotic zone in the EEP (Wells et al., 1995; Gordon et al., 1997; Kaupp et al., 2011). Continental shelf and fluvial fluxes of terrestrial material via surface and subsurface currents can deliver vast amounts of Fe and Al to the EUC at its origin around 150°E (Gordon et al., 1997; Wells et al., 1999; Mackey et al., 2002; Kaupp et al., 2011). The ratio of dFe to dAl in the EUC waters convinced Kaupp et al. (2011) that hydrothermal vents are an unlikely source of these elements for the EEP. Fluxes of dFe and dAl are expected to vary in strength at the EUC source, which will in turn be reflected in the magnitude of their upwelling flux and most likely in enhanced new production in the EEP (Slemons et al., 2009; Kaupp et al., 2011). The EB04 and EB05 cruises showed that the distribution of enhanced dFe and dAl coincides with the path of the EUC (Kaupp et al., 2011). It is speculated that this is even more pronounced in the western equatorial Pacific. West of 140°W, there is a significant reduction in dFe concentrations in surface waters (Kaupp et al., 2011). The different distributions of dFe and dAl in the EEP surface waters (Kaupp et al., 2011) could be attributed to preferential biological removal of dFe. Even though both dFe and dAl are scavenged onto particles, the differences in depth and rate of remineralization could explain the distinct vertical profiles of their concentrations.

Despite improvements in developing precise analytical methods for trace metal measurements, the limited spatial and temporal resolution of observations prevent the quantification of the physical transport of Fe. Studies of marine Fe biogeochemistry have therefore focused on either geochemical (Johnson et al., 1997; Martin et al., 1989; De Baar et al., 1995; Fung et al., 2000; Parekh et al., 2004) or biological aspects (Bowie et al., 2001;

Tortell et al., 1999; Price and Morel, 1998). Constructing Fe budgets has been hindered by the lack of estimates of several flux terms (e.g. Fe remineralization dynamics, particle sinking) (Boyd et al., 2005; Wu and Boyle, 2002; Fung et al., 2000). Iron removal is a function of many factors such as: biological uptake, number and size distributions of colloidal and small particles, aggregation processes and Fe ligand dynamics (Moore and Braucher, 2007). Because Fe removal rates are highly non-linear, especially in areas of high input fluxes, surface Fe concentrations are not good indicators of input and removal processes (Moore and Braucher, 2007). This feature stresses the need to study the aspects of biogeochemical cycling of trace elements from a flux rather than a reservoir perspective. A detailed biogeochemical flux budget was constrained under unperturbed conditions in a small patch of HNLC waters south east of New Zealand by Boyd et al. (2005). A simple budget for dFe was made by Landry et al. (1997) for the equatorial Pacific but it was based on few data points and several key assumptions that require revision.

In this paper we use a box model approach to calculate physical transports of dFe and dAl and constrain their biogeochemical budgets. This approach combines high-resolution circulation model velocity fields with dFe and dAl concentration from the EB04 and EB05 cruises. Through the application of a box model we estimate the average supply and removal rates within the EEP, which can potentially complement scarce *in situ* measurements of rate processes.

2. Methods

A box model was created and designed to constrain the flux budget of a chosen oceanographic property within a given area. Fig. 1 shows the extent of two large domains within the equatorial Pacific region delineated for the purpose of this study. The 'Wyrтки Box' encompasses the area between 180° and 90°W, and 5°S and 5°N. The 'EEP Box' represents the area between 140°W and 110°W with different meridional extents ranging from 0.5° to 4° around the equator. Based on the results of volume transport balance analysis, the vertical extent is set at the depth of 75 m (see Section 3.1.).

Flux budget calculations are based on the advection conservation equation of the following form:

$$\frac{\partial(uC)}{\partial x} + \frac{\partial(vC)}{\partial y} + \frac{\partial(wC)}{\partial z} = SUM \quad (1)$$

The flux term is defined as the spatial gradient of the product of velocity (zonal - u , meridional - v , or vertical - w) and a property concentration (C). The box model evaluates the sum of physical advective fluxes in- and out- of each side of a three-dimensional box. The transport at each wall is a surface integral of all fluxes measured along that side of the box, and the difference between the opposite sides of the box gives the net flux in that

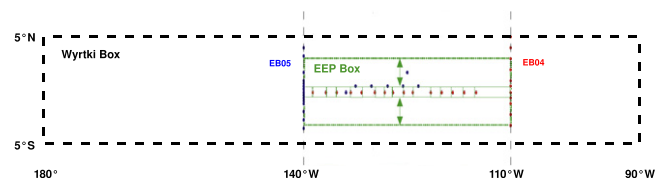


Fig. 1. The geographical extent of the two domains used in this study: the Wyrтки Box (black dotted) and the EEP Box (green dotted). Additionally, the EEP Box is divided into adjacent composite boxes. Their meridional extent is variable, as they stretch from 0.5° to 4° north and south of the equator (marked by green arrows). The sketch also displays the location of cruise stations from EB04 (red dots) and EB05 (blue dots), at which dFe and dAl concentration measurements were taken.

particular direction. Unless otherwise stated, fluxes are reported in units of concentration per meter squared per day. Under the assumption of steady-state conditions, the sum of the net physical fluxes is equal to the sum of biological and chemical fluxes.

The sum of net fluxes of a conservative property, such as volume transport or heat, needs to be conserved, *i.e.* the sum must equal zero. The sum of physical fluxes of a non-conservative element, such as NO_3 or dFe, should not be zero. Such flux budgets of non-conservative elements can therefore provide an implicit estimate of the net biogeochemical removal or regeneration. This estimate is conceptually equivalent to a Source Minus Sink (SMS) term used in ecosystem modeling.

In our calculations we do not include diffusive and atmospheric fluxes as physical supplies to the total budget. Diffusive fluxes in the EEP are small compared to advection (Chai et al., 1996) and are omitted here for simplicity. Although Aeolian deposition has typically been included in evaluating dFe and dAl budgets, we discard this term based on the results of Kaupp et al. (2011), who have shown that this flux is insignificant compared to the upwelling supply.

The box model's design is flexible enough to utilize various sources of data, such as model output and *in situ* data. Furthermore, it can be applied to any variable, or in another oceanic region for which measurements of velocity and concentration gradients exist. Flux calculations are programmed to handle data arranged on an irregular grid, as is often the case with shipboard-collected measurements. It is important to understand that this study is not a model simulation, rather, it is a budget calculation based on a comprehensive set of *in situ* observations and processed model outputs.

The suitability of the chosen approach is first validated by constraining the budgets controlled by physical processes alone: volume transport and heat. The calculations are repeated and compared for a series of boxes with different bottom depths - 50, 75 and 100 m - in order to optimize the advective flux balance while maintaining the strong upwelling signal in the results. Subsequent budget calculations based on modeled NO_3 and $\text{Si}(\text{OH})_4$ concentrations test the capability of the box model to estimate the rate of physical supply and removal through biogeochemical cycling. The same approach is then applied to $\text{NO}_3/\text{Si}(\text{OH})_4$, and dFe/dAl budgets by combining the observed concentration data from EB04 and EB05 cruises with the circulation model results.

The majority of oceanographic variables included in the model calculations are taken from the Regional Ocean Modeling System (ROMS) model coupled with the CoSiNE (Carbon, Silicate and Nitrogen Ecosystem) model (Chai et al., 2002, 2009; Dugdale et al., 2002a; Liu and Chai, 2009a, b). ROMS-CoSiNE is a multi-purpose, multi-disciplinary oceanic modeling tool that includes efficient physical and numerical algorithms and among others, a biogeochemical coupled model application. A basin-scale ROMS-CoSiNE has been developed for the Pacific Ocean with a spatial resolution of 12.5 and 50 km. The model has been forced with daily-averaged QuikScat surface winds (Xiu et al., 2010). In this study we use the following variables from the model output: x-, y- and z- momentum, potential temperature, NO_3 , $\text{Si}(\text{OH})_4$ (all at 12.5 km resolution) and surface heat flux. The *in situ* measurements of NO_3 , $\text{Si}(\text{OH})_4$, dFe and dAl concentrations were obtained from the EB04 and EB05 cruises aboard the R/V Roger Revelle. DFe was determined using the spectrophotometric flow injection analysis (Fe-FIA) method of Measures (1995), while dAl was determined using the fluorometric FIA (Al-FIA) method of Resing and Measures (1994). Details of sampling and analysis can be found in Kaupp et al. (2011). The protocol for collection and analysis of NO_3 and $\text{Si}(\text{OH})_4$ data is described in detail in Parker et al. (2011).

Because of the lack of time series measurements of either NO_3 and $\text{Si}(\text{OH})_4$, or dFe and dAl within the EEP, we cannot estimate the rate of change of concentration. The calculated budgets present a monthly snapshot of the processes taking place in the EEP and the biogeochemical conditions during the time the cruise data were collected. In contrast, budgets constrained from the Pacific ROMS-CoSiNE modeled data are based on the 2002–2005 monthly mean climatology. The rate of change of concentration is estimated for each month during the 4-year period, and this term is insignificant compared to all advective terms. In consequence, we assume that the system is in a steady-state condition in our calculations.

The variety of data types used in this study requires the adoption of flexible box schemes, whose spatial arrangements are presented in Fig. 1. Calculations involving only Pacific ROMS-CoSiNE model results are based on a single box configured for the Wyrтки Box or the EEP domain. The second calculation scheme is configured to match the regular model-derived velocity grid with the irregular *in situ* NO_3 and $\text{Si}(\text{OH})_4$ and dFe and dAl field data. Here we divide the EEP into a number of composite boxes, based on the locations of EB04 measurements. Although similar boxes can be drawn around the sites where EB05 data were collected, they do not cover the area east of 125°W and are difficult to compare with the EB04-based budgets. Strutton et al. (2011) analyzed the differences in hydrographic conditions between the two cruises in a great detail.

We furthermore estimate the NO_3 and $\text{Si}(\text{OH})_4$ flux balance based on the field-measured nutrient concentrations in order to evaluate how well the subsequent dFe and dAl composite budgets are constrained. While zonal and vertical concentration gradients are obtained from a number of along-equatorial stations, the meridional gradient is only available from the cross-equatorial sections at 110°W and 140°W from EB04 and EB05, respectively. We perform a study in which we compare three gradients from: 140°W , 110°W and the average of 140°W and 110°W , and assess the effect of applying different meridional gradients on the overall flux balance. Moreover, we test the sensitivity of the physical fluxes to changes in the box domain size. While the west and east walls remain fixed at 140°W and 110°W , respectively, the south and north sides of the EEP Box are adjusted between: 0.5°S and 0.5°N , 1°S and 1°N , 2°S and 2°N , 3°S and 3°N , and 4°S and 4°N . We refer to these configurations as EEP0, EEP1, EEP2, EEP3 and EEP4, respectively. The flexibility of the box domain provides an additional sensitivity measure on our calculations.

3. Results and discussion

In this section, we present and discuss the results of the flux budget calculations carried out according to the approach described in Section 2. It is divided into three subsections: (1) the volume transport and heat budget in the Wyrтки Box, (2) the NO_3 and $\text{Si}(\text{OH})_4$ budgets in the Wyrтки Box and the EEP region, (3) the dFe and dAl budgets in the EEP region.

3.1. Volume transport and heat budgets

We calculate volume transport and heat budgets to test whether the box model is capable of producing well-balanced advective fluxes.

The distribution of the net volume transport fluxes is shown in Fig. 2. The volume transport budget is based on the lateral (zonal and meridional) and vertical advective fluxes, all reported in Sv ($1 \text{ Sv} = 1 \times 10^6 \text{ m}^3 \text{ s}^{-1}$). The upwelling flux is the only net inflow into the Wyrтки Box and is approximately equal to 48 Sv, being in good agreement with the 50 Sv derived theoretically by Wyrтки

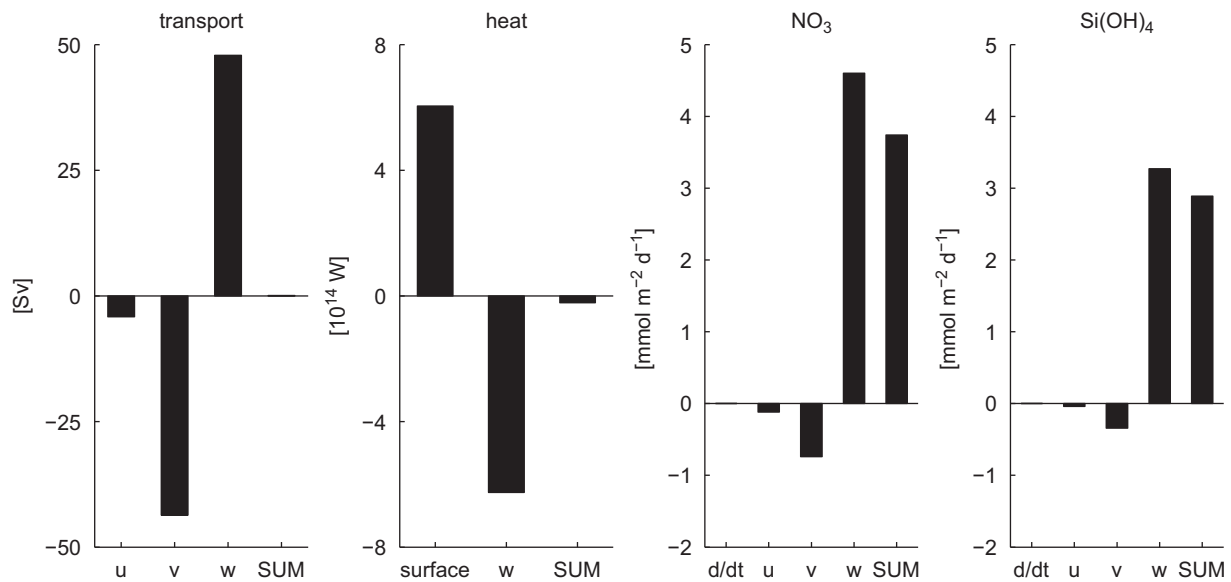


Fig. 2. The bar diagram presents the distribution of net advective fluxes of volume transport [Sv] and heat [10^{14} W] (left two panels), and NO_3 and $\text{Si}(\text{OH})_4$ [$\text{mmol m}^{-2} \text{d}^{-1}$] (right two panels) inside the Wyrтки Box. u represents the zonal, v the meridional, and w the vertical advection flux. In the heat budget, *surface* stands for the net surface heat flux and w is the vertical cooling due to the upwelling flux. In all budgets, the SUM represents the net sum of physical fluxes from and into the box (see Eq. (1)). The d/dt term represents the time rate of change of concentration in the NO_3 and $\text{Si}(\text{OH})_4$ budgets but is in both cases approximately equal to zero.

Table 1

Summary of the box model transport budget [Sv] compared with the results from Wyrтки (1981). Calculations were repeated at 50, 75 and 100 m depth selected as the bottom of the Wyrтки Box ($180\text{--}90^\circ\text{W}$, $5^\circ\text{S}\text{--}5^\circ\text{N}$). All data is obtained from the 2002–2005 monthly mean climatology Pacific ROMS-CoSiNE model results. w denotes the vertical velocity averaged over the Wyrтки Box at the given depth level. The error estimate expressed in % is derived from the ratio of the SUM flux to the highest advective flux in the budget.

Source	Depth [m]	w [10^{-4} m s^{-1}]	Transport flux [Sv]					Error [%]
			Zonal	Meridional	Vertical	SUM		
This study	50	0.22	−1.37	−47.22	47.13	−1.47	1.60	
	75	0.25	−4.16	−43.61	47.85	0.08	0.16	
	100	0.22	−8.27	−22.06	31.14	0.82	2.63	
Wyrтки (1981)	50	–	–	51	51	–	–	

(1981). The upwelling flux is balanced with 44 Sv and 4 Sv meridional and zonal outflow, respectively. The high ratio of north-south to east-west fluxes is comparable with the one calculated by Wyrтки (1981). The budget calculation is sensitive to the selection of the box bottom depth. Although Wyrтки (1981) chose 50 m as the bottom of his surface box, we find that the domain-averaged vertical velocity and vertical volume transport flux are both at a maximum using a depth of 75 m. More importantly however, when integrating over this depth, we achieve the optimum volume transport balance. Any imbalance expressed as a percentage of the highest advective flux term is most likely due to lack of mixing and sea-surface height gradient terms, which can alter the volume transport balance within the domain. Using a 75 m deep box, this imbalance equals 0.16%. All the volume transport budgets for the Wyrтки Box are listed in Table 1.

The results of the heat budget are also shown in Fig. 2. We evaluate the net heat fluxes against previously derived theoretical considerations. Wyrтки (1981) concluded that net surface heat gain (8.5×10^{14} W) is balanced with the cooling of upwelled water (-8.4×10^{14} W) in the equatorial upwelling zone. Our results confirm Wyrтки's hypothesis because of the balance between net surface heat gain of 6.04×10^{14} W and net cooling due to upwelling of -6.26×10^{14} W. When the box bottom is set at 75 m depth, the heat flux imbalance in our budget calculation

equals only 3.5%. This imbalance increases considerably when the depth is set to 50 m or 100 m, most likely due to the larger volume transport imbalance (see Table 1). In consequence, we have selected 75 m as the depth of the box bottom in all our subsequent budget calculations.

A similar advective flux balance analysis is applied within the EEP domain to establish the optimum size and number of composite boxes required to constrain budgets with unknown biogeochemical components. Based on the locations of the measurements we select 11 boxes for the NO_3 and $\text{Si}(\text{OH})_4$ and 8 boxes for the dFe and dAl budget, keeping each composite box at least 2° of longitude apart. Minimum volume transport imbalance is obtained for a $2^\circ\text{S}\text{--}2^\circ\text{N}$ meridional range when averaged over all composite boxes. In the case of the 11-box budget, the mean imbalance equals 4.74% with a standard deviation of 4.56%. The corresponding result for the 8-box configuration is $4.08 \pm 3.95\%$. In contrast, a narrower domain of $1^\circ\text{S} - 1^\circ\text{N}$ gives a mean imbalance of $7.79 \pm 5.24\%$ and $6.16 \pm 3.30\%$ for the 11-box and 8-box configurations, respectively. Similarly, a wider domain of $4^\circ\text{S}\text{--}4^\circ\text{N}$ results in a mean imbalance of $6.31 \pm 8.42\%$ and $6.06 \pm 7.95\%$ for the 11-box and 8-box schemes. For a narrower meridional range, the lateral heat flux becomes important, therefore the imbalance of the heat budget increases. However, a well-constrained volume transport budget is sufficient for our budget calculation purposes.

3.2. NO_3 and $\text{Si}(\text{OH})_4$ budgets

In order to expand the model evaluation, we test the capability of the box model approach to estimate the physical supply and biological/chemical removal and recycling of nutrients. We estimate NO_3 and $\text{Si}(\text{OH})_4$ budgets and compare them with the previous nutrient budget calculations in this area (Chai et al., 1996; Jiang et al., 2003). By doing so we demonstrate the usefulness of this nutrient balance calculation. In this study, we apply a number of different box model configurations in combination with observed nutrient concentration from various sources.

3.2.1. ROMS-CoSiNE budget

Firstly, we use the monthly averaged NO_3 and $\text{Si}(\text{OH})_4$ climatology concentration from the Pacific ROMS-CoSiNE model to constrain the budgets in the Wyrтки Box and in the EEP Box. Hereafter, we refer to these calculations as the ROMS-CoSiNE budget. Model-derived NO_3 and $\text{Si}(\text{OH})_4$ concentrations used in this box model were previously evaluated with *in situ* measurements in a number of model-data comparison studies (Jiang et al., 2003; Dugdale et al., 2007; Chai et al., 2007).

In the right two panels of Fig. 2 we present the distribution of net fluxes of NO_3 and $\text{Si}(\text{OH})_4$ within the Wyrтки Box. The vertical upwelling supply equals 4.60 and 3.27 $\text{mmol m}^{-2} \text{d}^{-1}$ of NO_3 and $\text{Si}(\text{OH})_4$, respectively. These upwelled nutrients are balanced partially with the meridional and zonal losses. Since NO_3 and $\text{Si}(\text{OH})_4$ are non-conservative in the ocean, the net sum of the advective physical fluxes indicates that biogeochemical processes need to be taken into account to maintain the nutrient balance under steady-state conditions. Hence, we infer that there is a net biological removal of 3.74 $\text{mmol m}^{-2} \text{d}^{-1}$ of NO_3 and 2.89 mmol of $\text{Si}(\text{OH})_4$ in the Wyrтки Box.

In the EEP Box, these uptake rates are higher and equal 4.74 $\text{mmol m}^{-2} \text{d}^{-1}$ NO_3 and 3.70 $\text{mmol m}^{-2} \text{d}^{-1}$ $\text{Si}(\text{OH})_4$, consistent with the proportionally higher vertical supply. These results are expected, *i.e.* higher average upwelling supply and enhanced biological productivity occur closer to the equator. Using a similar budget calculation, Jiang et al. (2003) estimated that NO_3 was removed at 2.01 $\text{mmol m}^{-2} \text{d}^{-1}$ in the Wyrтки Box and at a higher rate of 2.33 $\text{mmol m}^{-2} \text{d}^{-1}$ in the EEP Box. They also reported that the biological uptake of $\text{Si}(\text{OH})_4$ was at 2.37 $\text{mmol m}^{-2} \text{d}^{-1}$ in the Wyrтки Box and at 2.73 $\text{mmol m}^{-2} \text{d}^{-1}$ in the EEP Box (Jiang et al., 2003). The biological removal of NO_3 and $\text{Si}(\text{OH})_4$ changes from time to time in response to physical and biological conditions in the region. For instance, Wang et al. (2006) reported a range of 1–3.5 $\text{mmol m}^{-2} \text{d}^{-1}$ NO_3 uptake inside the Wyrтки Box. Nonetheless, when compared to a number of previous field and modeling studies in this region, our budgets tend to be higher for both NO_3 and $\text{Si}(\text{OH})_4$ uptake rates. In comparison with the previous study of Jiang et al. (2003), the higher uptake rates in this study are due to the overestimated vertical nutrient supply (Table 3). While our study uses the results from a much higher resolution model (12.5 km vs. 0.5° in latitude and 2° in longitude in Jiang et al. (2003)), it is difficult to conclude that this is the cause for the discrepancy between the two estimates.

We also evaluate the ROMS-CoSiNE budget by checking the Si:N ratios within the flux budgets. The vertical supply of $\text{Si}(\text{OH})_4$ is lower than NO_3 , with an Si:N ratio of 0.71. Meridional outflow of $\text{Si}(\text{OH})_4$ in the Wyrтки Box is also lower than that of NO_3 , reflecting the observed difference in concentration in the EEP surface waters (Strutton et al., 2011).

Our results show the low $\text{Si}(\text{OH})_4:\text{NO}_3$ ratio found in the EUC, the origin of which appears to be in the Southern Ocean (Dugdale

et al., 2002a), as well as the less efficient regeneration of $\text{Si}(\text{OH})_4$ within the upper water column of the equatorial Pacific (Jiang et al., 2003). Nevertheless, our ratio presents an underestimate with respect to the 0.85 ratio of Jiang et al. (2003) and 0.80 ratio of Ku et al. (1995). Consequently, the net Si:N removal ratio of 0.78 in the Wyrтки Box is slightly lower than 0.85 predicted by Jiang et al. (2003) and 0.83 reported by Chai et al. (2002). The fact that the uptake ratio is higher than the corresponding upwelling supply ratio points to $\text{Si}(\text{OH})_4$ being taken up more rapidly than NO_3 . This observation is consistent with the conclusions reached by Jiang et al. (2003).

3.2.2. ROMS-CoSiNE+EB budget

In order to evaluate the composite box scheme based on irregularly spaced concentration profiles, we combine NO_3 and $\text{Si}(\text{OH})_4$ measurements from EB04 and EB05 cruises with the monthly average 12.5 km velocity from the circulation model. We compare these results, which we refer to as the ROMS-CoSiNE+EB budget, with the ROMS-CoSiNE budget estimate. Finally, as an additional means of evaluating the box model approach, we provide the modeled nutrient uptake rates calculated by the Pacific ROMS-CoSiNE model explicitly.

Fig. 3 shows the mean SUM flux (defined in Eq. (1)) of NO_3 and $\text{Si}(\text{OH})_4$ from a standard EEP2 composite box configuration (top panels). Compared to the single box scheme, we obtain a similar balance between lateral and vertical fluxes resulting in net positive sum of physical fluxes. Higher meridional loss and upwelling supply are due to the differences in the latitudinal range of the two budgets. The net NO_3 removal rate equals 8.52 $\text{mmol m}^{-2} \text{d}^{-1}$ while the $\text{Si}(\text{OH})_4$ removal is estimated at 4.16 $\text{mmol m}^{-2} \text{d}^{-1}$. The calculated N:Si removal ratio of 2.05 is close to the reported mean of 1.83 for EB04 in December 2004 and 3.31 for EB05 in September 2005 between 1°S and 1°N (Dugdale et al., 2011). As the meridional extent of the composite box increases to 4°S–4°N (EEP4), mean removal rates decrease due to lower supply of nutrients via upwelling farther away from the equator. In this case, the NO_3 removal rate is 4.56 $\text{mmol m}^{-2} \text{d}^{-1}$, while the $\text{Si}(\text{OH})_4$ removal rate is 2.19 $\text{mmol m}^{-2} \text{d}^{-1}$ (Fig. 3). Although the meridional range of the EEP4 composite box domain is still smaller than the 5°S–5°N domain range adopted in the ROMS-CoSiNE budget, the removal rates of NO_3 from those two calculations are similar. This indicates that our method is robust considering that the observed and the modeled NO_3 concentrations are used in the calculations. On the other hand, the $\text{Si}(\text{OH})_4$ removal based on measured $\text{Si}(\text{OH})_4$ concentrations (4.16 $\text{mmol m}^{-2} \text{d}^{-1}$) is about twice that based on the modeled concentration field (2.37 $\text{mmol m}^{-2} \text{d}^{-1}$). We suspect that the greater disagreement between the various $\text{Si}(\text{OH})_4$ budget calculations is due to the larger difference in the $\text{Si}(\text{OH})_4$ concentration gradients obtained from the EB04/EB05 cruises and the Pacific ROMS-CoSiNE model.

Zonal distribution of the net NO_3 and $\text{Si}(\text{OH})_4$ fluxes is achieved through the composite box model arrangement. The top panel in Fig. 5 shows the net upwelling fluxes at 75 m depth in the 11 boxes that comprise the ROMS-CoSiNE+EB budget. The upwelling supply appears to be consistently high along the equator, which is to be expected in the domain that coincides with the equatorial upwelling zone. NO_3 is delivered at a rate ranging from 15 to 23 $\text{mmol m}^{-2} \text{d}^{-1}$, while $\text{Si}(\text{OH})_4$ delivery is 5–12 $\text{mmol m}^{-2} \text{d}^{-1}$. We suspect that the maximum vertical supply of NO_3 and $\text{Si}(\text{OH})_4$ between 130°W and 120°W is attributable to maximum vertical velocities found at 75 m depth within this longitude range (Chai et al., 1996). These high upwelling supplies of nutrients near the equator are removed by both the meridional and zonal transport. This means that the

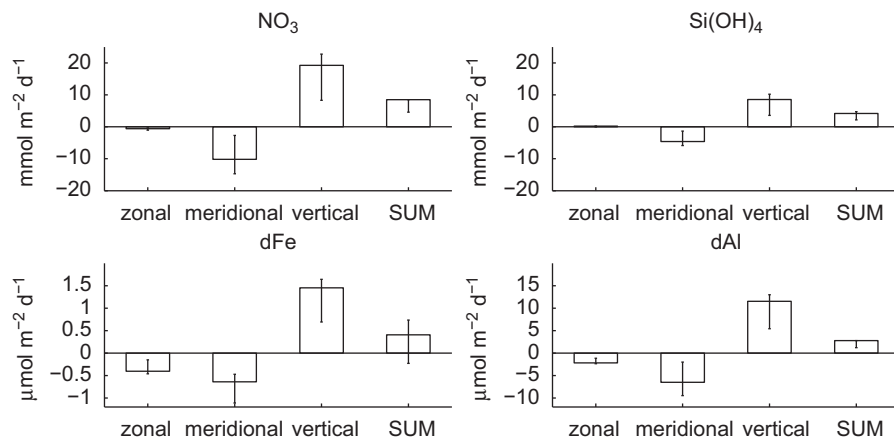


Fig. 3. Bar diagram shows the distribution of the mean EEP net fluxes of NO_3 and Si(OH)_4 [$\text{mmol m}^{-2} \text{d}^{-1}$] and dFe and dAl [$\mu\text{mol m}^{-2} \text{d}^{-1}$]. The net fluxes are averages from 11 and 8 composite boxes for $\text{NO}_3/\text{Si(OH)}_4$ and dFe/dAl , respectively. Flux calculations are based on the EB04 and EB05 concentration measurements. These results come from the EEP 2 box configuration, with the bottom depth of 75 m and meridional extent of 2°S – 2°N . Vertical lines added onto the bars represent the range of rate estimates obtained from calculations performed with wider or narrower meridional extent of the domain (ranging from EEP0 to EEP4).

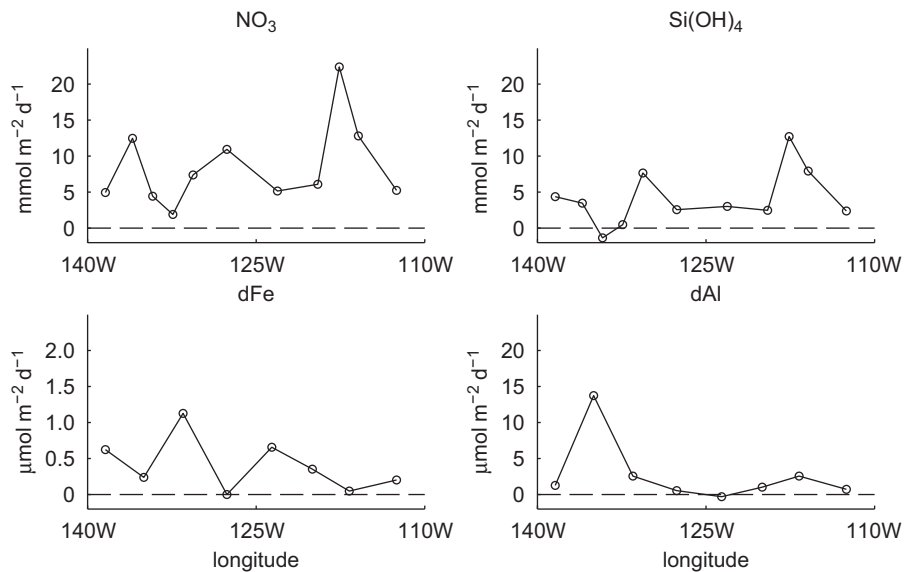


Fig. 4. Zonal distribution of the sum of net physical fluxes of NO_3 (top left), Si(OH)_4 (top right), dFe (bottom left) and dAl (bottom right) between 140°W and 110°W . The results come from composite box budgets from the EEP2 box configuration with a depth of 75 m and meridional extent of 2°S – 2°N .

net vertical nutrient flux into the surface zone is not equivalent to the flux of nutrients that is available to phytoplankton.

The net removal flux of both NO_3 and Si(OH)_4 exhibits greater zonal variability, with adjacent minima and maxima differing often by a factor of two (top panel in Fig. 4). We think that the spatial variability reflects the passage of a tropical instability wave (TIW) that was shown to affect nutrient concentrations and phytoplankton uptake rates during the equatorial transect of EB04 cruise (Strutton et al., 2011; Krause et al., 2011; Demarest et al., 2011; Dugdale et al., 2011; Kaupp et al., 2011; Parker et al., 2011). However, without more elaborate means of quantitative analysis, we cannot unambiguously relate the observed biogeochemical features to TIW activity.

In Table 3 we summarize all NO_3 and Si(OH)_4 flux results and compare them with various *in situ* and modeling supply and uptake rates of NO_3 and Si(OH)_4 published between 1992 and 2009. Although all cited studies were conducted in the equatorial Pacific, they are often characterized by different spatial and temporal scales of analysis. Moreover, they were carried out

under distinct hydrographic conditions determined by phenomena such as the El Niño Southern Oscillation (ENSO), Kelvin waves and TIWs. Therefore, the compilation of measurements in Table 3 represents a range of possible physical supply and biological uptakes occurring within the EEP domain.

Our box model budget calculations are in good agreement with the model estimates derived for the Wyrki Box and the eastern equatorial Pacific region (Chai et al., 1996; Jiang et al., 2003). Net NO_3 removal of $8.52 \text{ mmol m}^{-2} \text{d}^{-1}$ in the standard EEP2 box presents an overestimate with respect to *in situ* measured NO_3 uptake rates from the EB04 and EB05 cruises published by Dugdale et al. (2007, 2011). For all phytoplankton larger than $0.45 \mu\text{m}$, they report uptake rates of $3.31 \text{ mmol m}^{-2} \text{d}^{-1}$ during EB04 and $4.32 \text{ mmol m}^{-2} \text{d}^{-1}$ during EB05. Although the two-year average of $3.82 \text{ mmol m}^{-2} \text{d}^{-1}$ is close to our averaged ROMS-CoSiNE budget flux of $4.74 \text{ mmol m}^{-2} \text{d}^{-1}$, it is lower than the December 2004 average net removal rate of $8.52 \text{ mmol m}^{-2} \text{d}^{-1}$ obtained from the EEP2 budget. The Si(OH)_4 removal rate of $4.16 \text{ mmol m}^{-2} \text{d}^{-1}$ from the EEP2 box is a factor of two greater

than the cruise mean integrated (1°S – 1°N) estimates of $1.70 \pm 0.55 \text{ mmol m}^{-2} \text{ d}^{-1}$ for EB04 and $1.24 \pm 0.61 \text{ mmol m}^{-2} \text{ d}^{-1}$ for EB05 (Krause et al., 2011). While our results overestimate the supply and removal fluxes of $\text{Si}(\text{OH})_4$ compared to the conceptually most similar study of Jiang et al. (2003), they match very closely many previous observational and modeling results (Blain et al., 1997; Dugdale and Wilkerson, 1998; Leynaert et al., 2001).

Furthermore, we show a comparison with the area-averaged and depth-integrated nutrient uptake rates calculated directly from the Pacific ROMS-CoSiNE model. Uptake of NO_3 equals $5.62 \text{ mmol m}^{-2} \text{ d}^{-1}$ in December 2004 in the EEP, which is slightly more than the 4.56 calculated from the ROMS-CoSiNE EEPBudget. The model $\text{Si}(\text{OH})_4$ uptake equals $3.25 \text{ mmol m}^{-2} \text{ d}^{-1}$, which is in good agreement with 3.70 from the ROMS-CoSiNE budget. Although we were not able to calculate the model remineralization rates at this time, we can estimate the relative role of remineralization in the surface waters by referring to the results of Jiang et al. (2003). They reported the $\text{Si}(\text{OH})_4$ dissolution to be 30% of $\text{Si}(\text{OH})_4$ uptake and NO_3 regeneration of 16% of the uptake in the top 112 meters of the water column. While NO_3 remineralization is even less in the top 75 meters, it is likely to increase in the case of $\text{Si}(\text{OH})_4$. We thus assume that within the box model domain the effect of NO_3 regeneration is negligible but more significant in the case of the $\text{Si}(\text{OH})_4$. More complex biological cycling of $\text{Si}(\text{OH})_4$, especially the dissolution of its biogenic fraction that is dependant on the local biological activity, can cause a greater discrepancy between our $\text{Si}(\text{OH})_4$ removal estimates and those from previous studies. Nonetheless, with these assumptions, our net removal rates approximate reported rates of biological uptake to within about a factor of two.

Despite the fact that the lateral extent of the EEP2 budget is narrower than many previous studies performed in the eastern equatorial Pacific, we choose it as the standard box model domain based on our sensitivity study results. Firstly, we note that the volume transport imbalance in the EEP2 is only $4.74 \pm 4.56\%$, lower than in other box configurations. Secondly, in a narrower box, such as EEP2, we are dealing with a hydrographic setting that is upwelling-dominated and perhaps more uniform in its meridional nutrient concentration gradient (Chai et al., 2002; Jiang et al., 2003). This is important due to the lack of sufficient concentration measurements away from the equator and the need to be concerned with the effect of stronger meridional circulation outside of the equatorial upwelling zone. In the EEP2 box it is reasonable to assume that the volume transport imbalance of less than 10% and a constant meridional concentration gradient do not present a severe limitation to the use of the composite box model approach.

We conclude that the physical transports and biogeochemical cycling estimates based on modeled velocity and *in situ* NO_3 and $\text{Si}(\text{OH})_4$ concentrations demonstrate the usefulness of the box model approach. The general consistency of box model rate calculations with limited observations and the previous modeling studies indicates that, under the assumption of steady-state conditions, it is possible to approximate biological removal rates in the equatorial Pacific using an advective flux balance.

3.3. Dissolved Fe and Al budgets

In this section, we proceed to calculate the physical transport of dFe and the dAl, not previously performed in such detail in the equatorial Pacific or anywhere in the global ocean. We calculate the dFe and dAl budgets in the EEP using observational data collected during the EB04 and EB05 cruises in combination with the high-resolution circulation model results. The results

represent the December 2004 domain-averaged values obtained from the mean results of 8 composite boxes.

Fig. 3 shows the mean net flux distribution of dFe and dAl (bottom panels) from the EEP2 budget. In the EEP surface waters, net lateral (meridional+zonal) advection accounts for all the physical loss of both dFe and dAl, with the meridional flux being considerably larger than the zonal one. Meridional and zonal fluxes of NO_3 and $\text{Si}(\text{OH})_4$ reveal a similar pattern (top panels in Fig. 3). The supply is controlled by vertical advection and it is larger than the sum of all loss terms. As a result, the sum of physical fluxes (SUM in Fig. 3) is positive, which indicates that dFe and dAl, much like NO_3 and $\text{Si}(\text{OH})_4$, need to be removed through biological and chemical processes in order to maintain the steady-state condition. We estimate that the net removal of dFe is $0.41 \mu\text{mol m}^{-2} \text{ d}^{-1}$ and net removal of dAl is $2.77 \mu\text{mol m}^{-2} \text{ d}^{-1}$. Below, we discuss local patterns of circulation and biogeochemical cycling which explain the observed pattern of flux distribution showed in Fig. 3.

Firstly, in spite of a large surface concentration gradient between 140°W and 110°W (Table 2), there is little zonal inflow of these elements from west of 140°W into the box. This is because the majority of the eastward transport is due to the EUC, whose core lies much deeper than 75 m, especially in the western part of our EEP Box (Tsuchiya, 1975; Chai et al., 1996; Wells et al., 1999; Jiang et al., 2003).

Secondly, meridional outflow is affected by the combination of the concentration gradient between the north and south boundaries, and enhanced volume transport away from the equatorial divergence zone. The distribution of dFe and dAl concentrations and their gradients is showed in Table 2, which summarizes the EB04 and EB05 dFe and dAl measurements. It is possible we have overestimated the meridional flux contribution by applying a uniform meridional concentration gradient. The meridional outflow decreases as the north – south boundaries are moved farther away from the equator, *i.e.* in EEP3 and EEP4 budgets. In the standard EEP2 box, confined to the zone of maximum upwelling, we evaluate the sensitivity of our budget calculation

Table 2

dAl and dFe concentration values measured at 110°W during EB04 and at 140°W during EB05. The values are projected onto a regular grid. If there were no measurements at given depth levels, the nearest recording was used instead provided it as no more than 10 meters away from the selected depth layer.

Latitude	Depth [m]	dAl [nM]		dFe [nM]	
		EB04	EB05	EB04	EB05
4°S	10	–	1.35	–	0.25
	75	–	0.95	–	0.24
3°S	10	2.19	1.19	0.38	0.13
	75	2.50	1.21	0.36	0.12
2°S	10	2.96	1.65	0.27	0.08
	75	3.34	1.38	0.30	0.11
1°S	10	3.34	1.68	0.56	0.09
	75	5.51	1.79	0.87	0.08
0.5°S	10	3.18	1.74	0.45	0.08
	75	3.86	2.18	0.49	0.08
Equator	10	4.27	2.08	0.65	0.12
	75	5.96	3.91	0.48	0.08
0.5°N	10	2.94	2.23	0.22	0.08
	75	3.52	4.86	0.30	0.08
1°N	10	2.10	3.00	0.30	0.08
	75	3.03	2.38	0.29	0.83
2°N	10	2.06	1.84	0.44	0.08
	75	2.49	2.23	0.34	0.12
3°N	10	2.24	2.30	0.54	0.08
	75	2.91	1.54	0.52	0.08
4°N	10	3.28	1.46	1.30	0.08
	75	2.72	1.64	0.68	0.19

by applying different meridional gradients, i.e. along 140°W and 110°W, respectively. For example, in case of dFe, the outflow decreases by 43% when based on the 110°W meridional gradient, which is weaker compared to the one from 140°W. This change is less pronounced for dAl where the decrease is 33%. We acknowledge that 2011 could introduce a bias in our net physical transport estimates. However, it is expected that the mean of two gradients measured along 110°W and 140°W provides a good first order approximation.

Thirdly, it is the presence of upwelling conditions that makes vertical advection the dominant physical source. Its contribution depends on the relative position of the nutricline and the depth of the maximum vertical velocity. Here, the upwelling supply equals $1.45 \mu\text{mol m}^{-2} \text{d}^{-1}$ and $11.51 \mu\text{mol m}^{-2} \text{d}^{-1}$ for dFe and dAl, respectively. In Table 3, we compare our net physical dFe supply rate with a few previously published results. Landry et al. (1997) estimated the dFe upwelling flux at $0.12 \mu\text{mol m}^{-2} \text{d}^{-1}$ based on a single profile of dFe measured at 140°W. Fung et al. (2000) used the results of a global model simulation to constrain dFe fluxes also at 140°W and reported an upwelling flux of only $0.01 \mu\text{mol m}^{-2} \text{d}^{-1}$. Kaupp et al. (2011) estimate that there is $200 \mu\text{mol-Fe m}^{-2} \text{yr}^{-1}$ ($0.55 \mu\text{mol m}^{-2} \text{d}^{-1}$) delivered by upwelling to the EEP surface waters - three orders of magnitude more than by atmospheric deposition. Similarly, the upwelling supply flux of dAl is two orders of magnitude greater than from dust (Kaupp et al., 2011). Our flux of $1.45 \mu\text{mol m}^{-2} \text{d}^{-1}$ vertically upwelled at 75 m depth is 2.6 times greater than reported by Kaupp et al. (2011). Kaupp et al. (2011) base their estimates on the EB04 concentration gradient from a single point and vertical velocity from 125–175 m given by Chai et al. (1996). In this study, the vertical velocity comes from 75 m depth, where it is on average three times greater than elsewhere in the water column. Spatial gradients in concentration and velocity cause the upwelling supply rates to vary considerably with depth and longitude. Bottom left and right panels in Fig. 5 indicate up to a 4-fold difference in the magnitude of dFe and dAl upwelling supply at 75 m depth along the equator in the region. In this study we have used the same concentration data as Kaupp et al. (2011), thus the discrepancy in flux estimates shows the importance of accounting for spatial variability in vertical velocity. Regardless of the quantitative differences, both studies that use the EB cruise data confirm that the equatorial Pacific is one of the unique open ocean provinces that rely on the upwelling supply and not on Aeolian deposition as the main source of Fe (Duce and Tindale, 1991; Gordon et al., 1997; Wells et al., 1999; Ryan et al., 2006).

Bottom left and right panels in Fig. 4 show the zonal distribution of the sum of physical fluxes from adjacent composite boxes. There is a clear distinction between higher sum of physical fluxes in the western and much lower in the eastern part of the section, in line with the expectations based on the significant drop in dFe surface concentration described by Kaupp et al. (2011). East of 125°W, the net vertical flux (Fig. 5) is significantly smaller than at around 140°W, and the SUM flux is close to zero (Fig. 4). Even though the characteristic eastward shoaling of the EUC shifts the potential maximum upwelling flux towards shallower depths (Chai et al., 1996; Wells et al., 1999; Jiang et al., 2003), the parallel decrease in the dFe vertical gradient seems to be dominant and diminishes its upwelling supply. Our estimates of very low dFe net physical supply at 110°W should not nevertheless be interpreted as indicative of lack of biological uptake of dFe. It is important to keep in mind that our SUM flux is the product of scavenging minus remineralization. Phytoplankton growth, evident from Si(OH)_4 and NO_3 uptake rates measured close to 115°W (Dugdale et al., 2007, 2011; Krause et al., 2011; Parker et al. 2011), would not have occurred without any input of bioavailable Fe. Under low new dFe input conditions, regenerated Fe is expected

to serve as the main source of this uptake. Selph et al. (2011) showed significant recycling of autotrophic plankton by microzooplankton in the EEP and implying high Fe remineralization rates. Finally, Kaupp et al. (2011) concluded that there is additional particle scavenging of dFe occurring in surface waters around 110°W, where concentrations reach the detection limit. Additionally, the residence time of the dFe pool is very short, on the order of weeks. Our close to zero SUM flux can therefore suggest that surface waters experience an approximate balance between biological/chemical removal and remineralization of dFe.

Both dFe and dAl show similarities in their high sum of physical fluxes patterns within the 140–135°W range. There are elevated surface and subsurface concentrations of dFe and dAl (Kaupp et al., 2011), coinciding with large vertical supply flux. It is likely that the majority of the subsurface dFe is advected into this area by the EUC. However, we cannot verify this statement without parallel measurements in the western equatorial Pacific. Kaupp et al. (2011) provide a more elaborate discussion on the zonal advection sources of dFe and dAl into the EEP, also in reference to 2006 *in situ* measurements at 160°W. The simple explanation assumes that biological uptake of new Fe is far greater than of regenerated Fe, consistent with the high upwelling supply and exceptionally high sum of physical fluxes. The uncertainty is the contribution of geochemical scavenging to the net removal and how it varies along the equator. Most biogeochemical models with Fe cycling explicitly incorporate higher geochemical scavenging rates at dFe concentrations that exceed the 0.6 nM, or where there is abundant particulate material in the surface waters (Christian et al., 2002; Moore and Braucher, 2007). In the absence of comprehensive field measurements of this process, such theoretical assumptions prevail in most Fe cycling and budget considerations. The EB04 zonal distribution of dFe reveals elevated (around 0.6 nM and higher) dFe concentrations below 100 m depth, and shallower west of 130°W. By closing our box at the depth of 75 m, we are perhaps significantly decreasing the contribution of inorganic geochemical scavenging to the net dFe removal in most parts of the EEP. It is possible that in our box model calculations we have confined the flux budget to a biologically dominated system. By comparing dAl, dFe, NO_3 and Si(OH)_4 removal patterns we re-evaluate these conclusions.

While plankton actively take up dFe in the euphotic zone, dAl is thought to have little if any biological importance (Moran and Moore, 1992). Biological uptake of dAl was observed in culture-grown and coastal ocean environments (Stoffyn, 1979; Gehlen et al., 2002), but in the open ocean incorporating of dAl into diatom frustules is considered an abiotic process (Hydes, 1979; Dixit et al., 2001). Both Fe and Al are subject to geochemical scavenging onto particles in their dissolved phase. Johnson et al. (1997) concluded that both Fe and Al are heavily complexed in seawater and are therefore removed at a similar rate. However, Moore and Braucher (2007) have more recently described dFe and dAl to have very different particle scavenging rates. dFe is suspected to be scavenged approximately ten times faster than dAl under higher dFe concentration (above 0.6 nM) conditions. The zonal gradient of dFe in the EUC appears much greater than that of dAl, suggesting relatively larger loss terms of dFe west of 140°W.

Fig. 4 compares the zonal distribution of the sum of physical fluxes (assumed to be balanced by net biological/chemical removal) of dAl and dFe with that of NO_3 and Si(OH)_4 . The distribution of NO_3 and Si(OH)_4 uptake rates shows a more complex, irregular pattern than that of dFe and dAl. TIWs have been shown to play a great role in regulating the upwelling supply of nutrients in this region, for example by displacing it poleward (Strutton et al., 2001; Dugdale et al., 2002a; Krause et al., 2011; Demarest et al., 2011; Strutton et al., 2011). Adjacent

Table 3
Comparison of NO₃, Si(OH)₄ and dFe upwelling supply and uptake rate estimates in the Equatorial Pacific Ocean obtained from selected observational and modeling-based studies. Results from this study are in fact the sum of physical fluxes which we assume are equivalent to net biological removal.

Source	Location	NO ₃		Si(OH) ₄		Fe	
		Upwelling [mmol m ⁻² d ⁻¹]	Uptake [mmol m ⁻² d ⁻¹]	Upwelling [mmol m ⁻² d ⁻¹]	Uptake [mmol m ⁻² d ⁻¹]	Upwelling [mmol m ⁻² d ⁻¹]	Uptake [mmol m ⁻² d ⁻¹]
Dugdale et al. (1992)	WEC88		1.42				
Chai et al. (1996)	1D model		3.36				
Rodier and Le Borgne (1997)	FLUPAC		2.90				
Raimbault et al. (1999)	OLIPAC		1.87				
Dugdale et al. (2002b)	1D model		1.96–3.25				
Ku et al. (1995)	EqPac 1992	2.60		2.10			
Blain et al. (1997)	FLUPAC				1.94		
Leynaert et al. (2001)	EBENE				2.58		
Chai et al. (2002)	1D CoSiNE		1.96		1.64		
McCarthy et al. (1996)	JGOFS EQPAC		0.72–2.80				
Dugdale and Wilkerson (1998)	EQPAC+Si-cycle model	3.97	2.36	2.36	2.36		
Jiang et al. (2003)	NCOM+CoSiNE	2.80	2.01	2.53	2.31		
	NCOM+CoSiNE	2.95	2.33	2.51	2.73		
Wang et al. (2006)	coupled 3D model		1–3.5				
Dugdale et al. (2011)	EB04		3.31				
	EB05		4.11				
Krause et al., 2011	EB04				1.70		
	EB05				1.24		
Landry et al. (1997)	JGOFS EQPAC					0.12	0.12
Fung et al. (2000)	GCM	3.44				0.01	0.06
Kaupp et al. (2011)	EB04						0.55
This study	ROMS-CoSiNE	4.60	3.74	3.27	2.89		
	ROMS-CoSiNE+EB	19.27	8.52	8.53	4.16	1.45	0.41

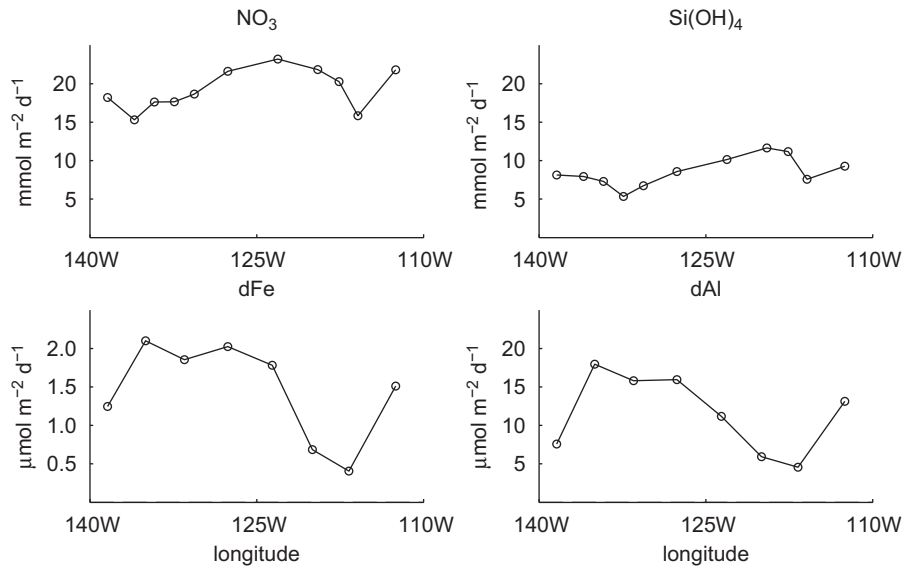


Fig. 5. Zonal distribution of the net upwelling supply fluxes NO₃ (top left), Si(OH)₄ (top right), dFe (bottom left) and dAl (bottom right) between 140°W and 110°W. The results come from the EEP2 composite box configuration.

minima and maxima in the sum of physical fluxes are apparent in the NO₃ and Si(OH)₄ flux distribution but also with dAl and dFe fluxes. For example around 115°W, they are possibly due to an intrusion of surface waters from south of the equator caused by a TIW. Kaupp et al. (2011) also present evidence for the low dAl input at 115°W.

Although biological/chemical cycling evidently plays a role in the zonal distribution of dFe and dAl fluxes, its signature is better displayed in the pattern of NO₃ and Si(OH)₄ fluxes. Fig. 5 in Dugdale et al. (2007) shows the EB04 size-fractionated NO₃ uptake rates along the equator, measured at 52%, 13% and 0.8% light depth. It appears that some areas of maximum net dFe removal match very well with the locations of maximum NO₃ uptake east of 140°W and around 125°W. Strutton et al. (2011) describe along-equator EB04 hydrographic profiles that reveal highest surface Si(OH)₄ concentrations roughly at the same longitudes. Parker et al. (2011) identified biological “hot spots” associated with TIW activity. In 2004, two of these hot spots with elevated Si(OH)₄ and NO₃ uptake were at 125°W and 135–140°W (their Figure 9) and correspond roughly with the western peaks in Fig. 4. Increased diatom uptake was found also in 2004 at 110°W. Si(OH)₄, much like dFe, is supplied via upwelling from the enriched EUC waters but its concentration is reduced to 1 or 2 μM in the surface waters (Ku et al., 1995). NO₃ on the other hand, is maintained at a relatively high level in the EEP, characteristic of the HNLC conditions. In a chemostat-like system, Si(OH)₄ might be the factor on which diatoms, that have a disproportionate role in the EEP new production (Krause et al., 2011), regulate their growth (Dugdale et al., 2002a, 2007, 2011).

Brzezinski et al. (2008) hypothesize that Fe-Si co-limitation is responsible for below maximum primary productivity in the EEP. Due to lack of direct measurements of dFe uptake, we cannot determine which element (Fe or Si) exerts a greater control on diatom growth. What is apparent is that where there is a significantly larger input of dFe, around 140–133°W (Fig. 5), NO₃ uptake rates reach their maxima in the EEP (Dugdale et al., 2007, 2011). Our composite NO₃ and Si(OH)₄ budget results reveal higher NO₃ and Si(OH)₄ removal in the central part of the domain where the strongest biological hot spots were found in both EB04 and EB05 by Parker et al. (2011). This discrepancy is again most likely due to the different time scales of analysis, in particular

related to the monthly-averaged velocity field used in our calculations. If TIWs control the supply and hence removal of nutrients in the EEP, then such a spatial mismatch between peak fluxes in our study and that of Dugdale et al. (2011) and Parker et al. (2011) can be attributed to a TIW shift in time. We conclude that Fe can potentially be limiting or co-limiting close to 110°W, where surface dFe concentration is close to detection limit (0.08 nM). It is not possible to conclude whether such conditions are permanent or transient due to a limited temporal resolution and the steady-state assumption. More detailed dFe measurements and improved flux estimates, both temporal and spatial, are required to resolve this issue.

Due to the steady-state assumption in our dFe and dAl budget calculations, we only report the domain-averaged sum of physical fluxes of dFe. This estimate is comparable with the results of dFe uptake rate from previous field and modeling studies included in Table 3. Landry et al. (1997) reported 0.12 μmol m⁻² d⁻¹ of Fe production and 0.01 μmol m⁻² d⁻¹ of Fe regeneration during the JGOFS EqPac Experiment. The latter flux was not measured but only calculated from the difference between Fe needed to support the measured rates of production and the rate of upwelling supply of new Fe. The flux difference between our 0.41 μmol m⁻² d⁻¹ and that of Landry et al. (1997) equal to 0.12 μmol m⁻² d⁻¹ comes from the lower dFe concentrations measured during the JGOFS study (Gordon et al., 1997). Given that very different approaches were used, there is a reasonable agreement between the rate estimates of biological removal of dFe with a range of 0.06–0.55 μmol m⁻² d⁻¹ compared to our estimate 0.41 μmol m⁻² d⁻¹ (Table 3). The efficient regeneration of dFe suggested by our results is also in agreement with the modeling study of Christian et al. (2002), who claimed that a one-way Fe path through the food web would result in a significant increase in the extent of the HNLC region in the equatorial Pacific. Fung et al. (2000) concluded that 30% of assimilated Fe at 140°W at the equator is supplied through recycling processes. However, their estimate came simply from the difference between total (new and recycled) assimilated and supplied dFe. As a result, their fluxes were considerably lower than in our study. The large quantitative discrepancy might originate from the fact that Fung et al. (2000) considered the Aeolian flux of Fe to constitute half the upwelling flux - an estimate that is inconsistent with data of

Kaupp et al. (2011). What is more, they verified their model against JGOFS concentrations from 140°W, which were much lower than those observed during EB04 and EB05. Finally, their study estimated Fe fluxes based on a predefined Fe:C ratio that is known to be highly variable, both in time and space.

Although the pelagic budget of dFe from Boyd et al. (2005) comes from another HNCL province, south east of New Zealand in the Southern Ocean, it is included in the comparison because it is the only similar comprehensive attempt to quantify the rate of biological uptake of dFe under natural conditions. Boyd et al. (2005) report biological uptake of dFe equal to 2.45–4.06 $\mu\text{mol m}^{-2} \text{d}^{-1}$, biological remineralization rate exceeding 1.98 $\mu\text{mol m}^{-2} \text{d}^{-1}$, and the geochemical scavenging, although not directly measured, of 0.22–0.55 $\mu\text{mol m}^{-2} \text{d}^{-1}$. An order of magnitude agreement between these measurements and our budget calculations is perceived as an additional independent evaluation of the approach used in this study.

The calculation of dFe:C flux ratio becomes an additional way of evaluating the flux budget. When evaluating these ratios, we restrict ourselves to a single domain-averaged estimate. In constructing the dFe:C ratio, we combine carbon uptake or primary productivity measurements from a number of literature sources (see Table 4) with our sum of physical fluxes of dFe. In our dFe:N ratio, we use the box model estimated net physical flux of both elements. The dFe:C ratio is traditionally used as an indicator of the degree of Fe limitation in the upper water column; however, it often derives from a product of cell quota measurements rather than community flux estimates (e.g. Twining et al., 2004).

In Table 4 we compare our estimates with those derived or applied in previous observational, laboratory and modeling studies. Our 3–9 $\mu\text{mol}:\text{mol}$ dFe:C ratio lies within the broad range of published values and is in good agreement with recent cell uptake rates measured in HNLC waters (Twining et al., 2004, 2011). The box model-derived sum of physical fluxes of dFe combines biological uptake, remineralization and scavenging processes, and so cannot be used to report dFe:C ratios separately for new and regenerated production. Therefore, we consider the dFe:C ratio analysis only as an additional way of evaluating our calculations. Namely, a close match between the calculated and

previously published ratios suggests that the majority of our net dFe removal is likely due to biological uptake. Had our ratio been much higher than the cell-based uptake estimate, we would have concluded there was a greater geochemical scavenging component in the total dFe removal flux.

There are some limitations that impose restrictions on interpreting the results of these box model calculations. Firstly, it appears that all four biogeochemical budgets discussed above show signs of large spatial variability. However, it is important to remember that all the sampling during the EB04 and EB05 cruises occurred over a span of 2–3 weeks and any spatial variability could in fact be due to potential change in concentration and/or flux. The observed passage of the TIW might have added to this uncertainty. However, due to the fact that a typical TIW has a much longer period (10 to 50 days, e.g. Halpern et al., 1988; Strutton et al., 2001) than our field sampling along the equator, the location of distinct maxima and minima should not have shifted significantly in space during the sampling period. Parallel analysis of the 12.5 km Pacific ROMS-CoSiNE model NO_3 and $\text{Si}(\text{OH})_4$ uptake rates confirms the existence of wave-like features that are most likely attributed to a passing TIW (Palacz et al., unpublished).

Further uncertainties in our calculations may originate from other assumptions. Firstly, we do not consider any mixing fluxes in our budgets, and although they are unlikely to alter the volume transport and heat balance in the Wyrcki Box, they could play a role in the dFe and dAl budgets in the EEP Box. Secondly, we have opted to neglect the atmospheric deposition of dFe and dAl. This assumption is based on the calculations of Kaupp et al. (2011) who compared the upwelling flux with the atmospheric deposition rates from the Measurement of Al for Dust Calculation in Oceanic Waters (MADCOW) model, developed by Measures and Brown (1996). An atmospheric deposition flux was included in previous attempts to construct the Fe budget in the equatorial Pacific, but was found to be insignificant compared to the upwelling flux by most studies (Landry et al., 1997; Christian et al., 2002; Moore et al., 2004), except for that by Fung et al. (2000).

Lastly, it must be kept in mind that our box model budgets do not evaluate the role particulate Fe (pFe) pool might have on the overall biogeochemical cycling of dFe. The main process that is possibly omitted this way is the photo-oxidation of pFe (Johnson et al., 1994; Miller et al., 1995). Even though solubilized pFe is said not to be part of the dissolved pool, it can support the growth of the plankton community (Johnson et al., 1997), and thus alter the estimated dFe:C uptake ratio.

Table 4

Comparison of dFe:N and dFe:C ratios from this study and ones reported in the literature. dFe and NO_3 values from this study are the sum of physical fluxes. Nitrogen and carbon flux values are obtained from previous studies, and represent nutrient uptake or productivity estimates. Any indirect conversions between Fe, N and C are based on the C:N Redfield ratio varying from 6.6 to 7.3.

Source	Fe:N $\mu\text{mol}:\text{mol}$	Fe:C $\mu\text{mol}:\text{mol}$
Morel and Hudson (1985)	46–660	7–100
Martin et al. (1989)	132–218	20–33
Price et al. (1994)	812–884	123–134
Coale et al. (1996)	66	10
Johnson et al. (1997)	33	5
Fung et al. (2000)	17	2.5
Christian et al. (2002)	200–33	3–5
Moore et al., 2004	40	6
Twining et al. (2004)	Unfertilized	– 6–14
	Fe-fertilized	– 10–40
Frew et al. (2006)	264	40
This study	^a 8.52 mmol-N $\text{m}^{-2} \text{d}^{-1}$	48
	^b 60–130 mmol-C $\text{m}^{-2} \text{d}^{-1}$	21–49
	^c 54 mmol-C $\text{m}^{-2} \text{d}^{-1}$	56
	^d 45 mmol-C $\text{m}^{-2} \text{d}^{-1}$	63

^a From Box EEP SUM of NO_3 .

^b From Barber et al. (1996).

^c From Pennington et al. (2006).

^d From Behrenfeld and Falkowski (1997).

4. Summary

In this study we present the results of a new box model approach to calculate physical transports and flux budgets of NO_3 , $\text{Si}(\text{OH})_4$ and dFe and dAl in the equatorial Pacific. We first successfully reconstruct the volume transport and heat budgets initially constrained by Wyrcki (1981). Furthermore, we calculate the sum of physical fluxes of NO_3 and $\text{Si}(\text{OH})_4$ and balance it with net biological uptake. Finally, we construct the most complete pelagic budget of dFe and dAl for the HNLC waters in the equatorial Pacific. Our results confirm that upwelling is by far the most significant source of dFe and dAl into the surface waters. By analyzing the zonal distribution of the sum of physical fluxes we show some of the spatial variability in net dFe and dAl removal, and link it to similar observed patterns in NO_3 and $\text{Si}(\text{OH})_4$ uptake rates. The budget calculations also partially support the Fe-limitation in the EEP, especially where the dFe concentrations and supply fluxes are low.

Comparison with previous observational and modeling studies reveal that our box model tends to overestimate the removal rates of NO_3 and $\text{Si}(\text{OH})_4$. This suggests that our calculated dFe and dAl fluxes present upper estimates. The assumption of steady-state conditions and lack of sufficient measurements of meridional concentration gradients are the main limitations of this study. Even so, the flexible design of the box model as well as the various sources of data used allowed for a very thorough study of fluxes and how they differ spatially within the equatorial Pacific.

Furthermore, we would like to point out that even though the box model relies on *in situ* measurements, it can be used to complement the logistically challenging rate measurements. Another advantage of this box model approach is that it can be applied and tested in other HNLC regions. The possibility of merging data sets in budget calculations offers a valuable means in process-oriented studies and can help remedy the problem of insufficient spatial and temporal coverage of field measurements. This aspect is of particular importance to the analysis of dFe and dAl fluxes and their role in the biogeochemical studies. With the start of the GEOTRACES program (<http://www.ldeo.columbia.edu/res/pi/geotraces>), we look forward to further evaluate the box budget approach and shed more light on the biogeochemistry of Fe and its link to the global carbon cycle.

Acknowledgments

This work is supported by grants from the National Science Foundation and National Aeronautics and Space Administration. The authors would like to thank Dr. Lei Shi for his assistance in processing the Pacific ROMS-CoSiNE model results. We are grateful to Drs. Huijie Xue, Mark Wells, Mary Jane Perry and Pete Strutton for comments on the box model design. We would further like to thank Dr. Frances Wilkerson and two anonymous reviewers for their many constructive suggestions that greatly improved an earlier version of this paper.

References

- Baines, S.B., Twining, B.S., Vogt, S., Balch, W.M., Fisher, N.S., Nelson, D.M., 2011. Elemental composition of equatorial Pacific diatoms exposed to additions of silicic acid and iron. *Deep-Sea Research II* 58 (3–4), 512–523.
- Balch, W.M., Poulton, A.J., Drapeau, D.T., Bowler, B.C., Windecker, L.A., Booth, E.S., 2011. Zonal and meridional patterns of phytoplankton biomass and carbon fixation in the equatorial Pacific Ocean between 110°W and 140°W. *Deep-Sea Research II* 58 (3–4), 400–416.
- Barber, R., Chavez, F., 1991. Regulation of primary productivity rate in the equatorial Pacific. *Limnology and Oceanography* 36 (8), 1803–1815.
- Barber, R., Sanderson, M., Lindley, S., Chai, F., Newton, J., Trees, C., Foley, D., Chavez, F., 1996. Primary productivity and its regulation in the equatorial Pacific during and following the 1991–1992 El Niño. *Deep-Sea Research II* 43 (4–6), 933–969.
- Behrenfeld, M., Falkowski, P., 1997. Photosynthetic rates derived from satellite-based chlorophyll concentration. *Limnology and Oceanography* 42 (1), 1–20.
- Blain, S., Leynaert, A., Treguer, P., Chretiennot-Dinet, M., Rodier, M., 1997. Biomass, growth rates and limitation of equatorial Pacific diatoms. *Deep-Sea Research I* 44 (7), 1255–1275.
- Bowie, A., Maldonado, M., Frew, R., Croot, P., Achterberg, E., Mantoura, R., Worsfold, P., Law, C., Boyd, P., 2001. The fate of added iron during a mesoscale fertilisation experiment in the Southern Ocean. *Deep-Sea Research II* 48 (11–12), 2703–2743.
- Boyd, P., 2002. The role of iron in the biogeochemistry of the Southern Ocean and equatorial Pacific: a comparison of *in situ* iron enrichments. *Deep-Sea Research II* 49 (9–10), 1803–1821.
- Boyd, P., Law, C., Hutchins, D., Abraham, E., Croot, P., Ellwood, M., Frew, R., Hadfield, M., Hall, J., Handy, S., Hare, C., Higgins, J., Hill, P., Hunter, K., LeBlanc, K., Maldonado, M., McKay, R., Mioni, C., Oliver, M., Pickmere, S., Pinkerton, M., Safi, K., Sander, S., Sanudo-Wilhelmy, S., Smith, M., Strzepek, R., Tovar-Sanchez, A., Wilhelm, S., 2005. FeCycle: attempting an iron biogeochemical budget from a mesoscale SF_6 tracer experiment in unperturbed low iron waters. *Global Biogeochemical Cycles* 19, 4.
- Bruland, K.W., Rue, E.L., Smith, G.J., 2001. Iron and macronutrients in California coastal upwelling regimes: implications for diatom blooms. *Limnology and Oceanography* 46 (7), 1661–1674.
- Brzezinski, M.A., Dumousseaud, C., Krause, J.W., Measures, C.I., Nelson, D.M., 2008. Iron and silicic acid concentrations together regulate Si uptake in the equatorial Pacific Ocean. *Limnology and Oceanography* 53 (3), 875–889.
- Brzezinski, M.A., Baines, S., Balch, W.M., Beucher, C., Chai, F., Dugdale, R.C., Krause, J.W., Landry, M.R., Marchi, A., Measures, C., Nelson, D.M., Parker, A., Selph, K.E., Strutton, P., Taylor, A.G., Twining, B., 2011. Co-limitation of diatoms by iron and silicic acid in the equatorial Pacific. *Deep-Sea Research II* 58 (3–4), 493–511.
- Chai, F., Lindley, S.T., Barber, R.T., 1996. Origin and maintenance of a high nitrate condition in the equatorial Pacific. *Deep-Sea Research II* 43 (4–6), 1031–1064.
- Chai, F., Dugdale, R., Peng, T.-H., Wilkerson, F., Barber, R., 2002. One-dimensional ecosystem model of the equatorial Pacific upwelling system. Part I: model development and silicon and nitrogen cycle. *Deep-Sea Research II* 49, 2713–2745.
- Chai, F., Jiang, M.-S., Chao, Y., Dugdale, R., Chavez, F., Barber, R.T., 2007. Modeling responses of diatom productivity and biogenic silica export to iron enrichment in the equatorial Pacific Ocean. *Global Biogeochemical Cycles* 21, 3.
- Chai, F., Liu, G., Xue, H., Shi, L., Chao, Y., Tseng, C.M., Chou, W.C., Liu, K.K., 2009. Seasonal and interannual variability of carbon cycle in South China Sea: a three-dimensional physical–biogeochemical modeling study. *Journal of Oceanography* 65 (5), 703–720.
- Chase, Z., Price, N., 1997. Metabolic consequences of iron deficiency in heterotrophic marine protozoa. *Limnology and Oceanography* 42 (8), 1673–1684.
- Chavez, F.P., Buck, K.R., Coale, K.H., Martin, J.H., Ditullio, G.R., Welschmeyer, N.A., Jacobson, A.C., Barber, R.T., 1991. Growth rates, grazing, sinking, and iron limitation of equatorial Pacific phytoplankton. *Limnology and Oceanography* 36 (8), 1816–1833.
- Christian, J., Verschell, M., Murtugudde, R., Busalacchi, A., McClain, C., 2002. Biogeochemical modelling of the tropical Pacific Ocean. II: Iron biogeochemistry. *Deep-Sea Research II* 49 (1–3), 545–565.
- Coale, K.H., 1991. Effects of iron, manganese, copper, and zinc enrichments on productivity and biomass in the sub-arctic Pacific. *Limnology and Oceanography* 36 (8), 1851–1864.
- Coale, K.H., Fitzwater, S.E., Gordon, R.M., Johnson, K.S., Barber, R.T., 1996. Control of community growth and export production by upwelled iron in the equatorial Pacific ocean. *Nature* 379 (6566), 621–624.
- Cullen, J.J., Lewis, M., Davis, C., Barber, R., 1992. Photosynthetic characteristics and estimated growth rates indicate grazing is the proximate control of primary production in the equatorial Pacific. *Journal of Geophysical Research* 97, 639–654.
- De Baar, H., De Jong, J., Bakker, D., Loscher, B., Veth, C., Bathmann, U., Smetacek, V., 1995. Importance of iron for plankton blooms and carbon dioxide drawdown in the Southern Ocean. *Nature* 373 (6513), 412–415.
- Demarest, M.S., Brzezinski, M.A., Nelson, D.M., Krause, J.W., Jones, J.L., Beucher, C., 2011. Net biogenic silica production and nitrate regeneration determine the strength of the silica pump in the eastern equatorial Pacific. *Deep-Sea Research II* 58 (3–4), 462–476.
- Dixit, S., Van Cappellen, P., van Bennekom, A.J., 2001. Processes controlling solubility of biogenic silica and pore water build-up of silicic acid in marine sediments. *Marine Chemistry* 73 (3–4), 333–352.
- Duce, R.A., Tindale, N.W., 1991. Atmospheric transport of iron and its deposition in the ocean. *Limnology and Oceanography* 36 (8), 1715–1726.
- Dugdale, R.C., Wilkerson, F.P., Barber, R.T., Chavez, F.P., 1992. Estimating new production in the equatorial Pacific ocean at 150°W. *Journal of Geophysical Research—Oceans* 97 (C1), 681–686.
- Dugdale, R.C., Wilkerson, F.P., 1998. Silicate regulation of new production in the equatorial Pacific upwelling. *Nature* 391 (6664), 270–273.
- Dugdale, R., Wischmeyer, A., Wilkerson, F., Barber, R., Chai, F., Jiang, M., Peng, T., 2002a. Meridional asymmetry of source nutrients to the equatorial Pacific upwelling ecosystem and its potential impact on ocean-atmosphere CO_2 flux; a data and modeling approach. *Deep-Sea Research II* 49 (13–14), 2513–2531.
- Dugdale, R.C., Barber, R.T., Chai, F., Peng, T.H., Wilkerson, F.P., 2002b. One-dimensional ecosystem model of the equatorial Pacific upwelling system. Part II: sensitivity analysis and comparison with JGOFS EqPac data. *Deep-Sea Research II* 49 (13–14), 2747–2768.
- Dugdale, R.C., Wilkerson, F.P., Chai, F., Feely, R., 2007. Size-fractionated nitrogen uptake measurements in the equatorial Pacific and confirmation of the low-Si high-nitrate low-chlorophyll condition. *Global Biogeochemical Cycles* 21, 2.
- Dugdale, R.C., Chai, F., Feely, R.A., Measures, C.I., Parker, A.E., Wilkerson, F.P., 2011. The regulation of equatorial Pacific new production and $p\text{CO}_2$ by silicate-limited diatoms. *Deep-Sea Research II* 58 (3–4), 477–492.
- Feely, R., Wanninkhof, R., Takahashi, T., Tans, P., 1999. Influence of El Niño on the equatorial Pacific contribution to atmospheric CO_2 accumulation. *Nature* 398 (6728), 597–601.
- Frew, R., Hutchins, D., Nodder, S., Sanudo-Wilhelmy, S., Tovar-Sanchez, A., LeBlanc, K., Hare, C., Boyd, P., 2006. Particulate iron dynamics during FeCycle in subantarctic waters southeast of New Zealand. *Global Biogeochemical Cycles* 20, 1.
- Frost, B.W., 1991. The role of grazing in nutrient-rich areas of the open sea. *Limnology and Oceanography* 36, 1616–1630.
- Fung, I., Meyn, S., Tegen, I., Doney, S., John, J., Bishop, J., 2000. Iron supply and demand in the upper ocean. *Global Biogeochemical Cycles* 14 (1), 281–295.
- Gehlen, M., Beck, L., Calas, G., Flank, A.M., Van Bennekom, A.J., Van Beusekom, J.E.E., 2002. Unraveling the atomic structure of biogenic silica: Evidence of the

- structural association of Al and Si in diatom frustules. *Geochimica et Cosmochimica Acta* 66 (9), 1601–1609.
- Gordon, R.M., Coale, K.H., Johnson, K.S., 1997. Iron distributions in the equatorial Pacific: implications for new production. *Limnology and Oceanography* 42 (3), 419–431.
- Gorgues, T., Menkes, C., Slemmons, L., Aumont, O., Dandonneau, Y., Radenac, M.H., Alvain, S., Moulin, C., 2010. Revisiting the La Nina 1998 phytoplankton blooms in the equatorial Pacific. *Deep-Sea Research I* 57 (4), 567–576.
- Greene, R., Kolber, Z., Swift, D., Tindale, N., Falkowski, P., 1994. Physiological limitation of phytoplankton photosynthesis in the eastern equatorial Pacific determined from variability in the quantum yield of fluorescence. *Limnology and Oceanography* 39 (5), 1061–1074.
- Halpern, D., Knox, R., Luther, D., 1988. Observations of 20-day period meridional current oscillations in the upper ocean along the Pacific equator. *Journal of Physical Oceanography* 18, 1514–1534.
- Hydes, D.J., 1979. Aluminum in seawater—control by inorganic processes. *Science* 205 (4412), 1260–1262.
- Jiang, M.S., Chai, F., Dugdale, R.C., Wilkerson, F.P., Peng, T.H., Barber, R.T., 2003. A nitrate and silicate budget in the equatorial Pacific Ocean: a coupled physical–biological model study. *Deep-Sea Research II* 50 (22–26), 2971–2996.
- Johnson, K.S., Coale, K.H., Elrod, V.A., Tindale, N.W., 1994. Iron photo-chemistry in seawater from the equatorial Pacific. *Marine Chemistry* 46 (4), 319–334.
- Johnson, K., Gordon, R., Coale, K., 1997. What controls dissolved iron concentrations in the world ocean? *Marine Chemistry* 57 (3–4) 137–161.
- Kaupp, L.J., Measures, C.I., Selph, K.E., Mackenzie, F.T., 2011. The distribution of dissolved Fe and Al in the upper waters of the eastern equatorial Pacific. *Deep-Sea Research II* 58 (3–4), 296–310.
- Krause, J.W., Nelson, D.M., Brzezinski, M.A., 2011. Biogenic silica production and the diatom contribution to primary production and nitrate uptake in the eastern equatorial Pacific Ocean. *Deep-Sea Research II* 58 (3–4), 434–448.
- Ku, T., Luo, S., Kusakabe, M., Bishop, J., 1995. Ra^{228} -derived nutrient budgets in the upper equatorial Pacific and the role of new silicate in limiting productivity. *Deep-Sea Research II* 42 (2–3), 479–497.
- Landry, M.R., Barber, R.T., Bidigare, R.R., Chai, F., Coale, K.H., Dam, H.G., Lewis, M.R., Lindley, S.T., McCarthy, J.J., Roman, M.R., Stoecker, D.K., Verity, P.G., White, J.R., 1997. Iron and grazing constraints on primary production in the central equatorial Pacific: an EqPac synthesis. *Limnology and Oceanography* 42 (3), 405–418.
- Leynaert, A., Treguer, P., Lancelot, C., Rodier, M., 2001. Silicon limitation of biogenic silica production in the equatorial Pacific. *Deep-Sea Research I* 48 (3), 639–660.
- Liu, G., Chai, F., 2009a. Seasonal and interannual variability of primary and export production in the South China Sea: a three-dimensional physical biogeochemical model study. *Journal of Marine Science* 66, 420–431.
- Liu, G., Chai, F., 2009b. Seasonal and interannual variation of physical and biological processes during 1994–2001 in the Sea of Japan/East Sea: a three-dimensional physical–biogeochemical modeling study. *Journal of Marine Systems* 78 (2), 265–277.
- Mackey, D.J., O'Sullivan, J.E., Watson, R.J., 2002. Iron in the western Pacific: a riverine or hydrothermal source for iron in the Equatorial Undercurrent? *Deep-Sea Research Part I—Oceanographic Research Papers* 49 (5) 877–893.
- Macrellis, H.M., Trick, C.G., Rue, E.L., Smith, G., Bruland, K.W., 2001. Collection and detection of natural iron-binding ligands from seawater. *Marine Chemistry* 76 (3), 175–187.
- Martin, J.H., Fitzwater, S.E., 1988. Iron-deficiency limits phytoplankton growth in the northeast Pacific subarctic. *Nature* 331 (6154), 341–343.
- Martin, J.H., Gordon, R.M., Fitzwater, S., Broenkow, W.W., 1989. Vertex—phytoplankton iron studies in the Gulf of Alaska. *Deep-Sea Research I* 36 (5), 649.
- Martin, J.H., Fitzwater, S.E., Gordon, R.M., 1990. Iron deficiency limits phytoplankton growth in Antarctic waters. *Global Biogeochemical Cycles* 4, 5–12.
- Martin, J.H., Gordon, R.M., Fitzwater, S.E., 1991. The case for iron. *Limnology and Oceanography* 36 (8), 1793–1802.
- Martin, J.H., Coale, K.H., Johnson, K.S., Fitzwater, S.E., Gordon, R.M., Tanner, S.J., Hunter, C.N., Elrod, V.A., Nowicki, J.L., Coley, T.L., Barber, R.T., Lindley, S., Watson, A.J., Vanscoy, K., Law, C.S., Liddicoat, M.I., Ling, R., Stanton, T., Stockel, J., Collins, C., Anderson, A., Bidigare, R., Ondrusek, M., Latasa, M., Millero, F.J., Lee, K., Yao, W., Zhang, J.Z., Friederich, G., Sakamoto, C., Chavez, F., Buck, K., Kolber, Z., Greene, R., Falkowski, P., Chisholm, S.W., Hoge, F., Swift, R., Yungel, J., Turner, S., Nightingale, P., Hatton, A., Liss, P., Tindale, N.W., 1994. Testing the iron hypothesis in ecosystems of the equatorial Pacific Ocean. *Nature* 371 (6493), 123–129.
- McCarthy, J., Garside, C., Nevins, J., Barber, R., 1996. New production along 140°W in the equatorial Pacific during and following the 1992 El Niño event. *Deep-Sea Research II* 43 (4–6), 1065–1093.
- Measures, C.I., 1995. The distribution of Al in the IOC stations of the eastern Atlantic between 30°S and 34°N. *Marine Chemistry* 49 (4), 267–281.
- Measures, C.I., Brown, E.T., 1996. Estimating dust input to the Atlantic Ocean using surface water aluminum concentrations. In: Geurzoni, S., Chester, R. (Eds.), *The Impact of African Dust Across the Mediterranean*. Springer, New York, pp. 301–311.
- Miller, W.L., King, D.W., Lin, J., Kester, D.R., 1995. Photochemical redox cycling of iron in coastal seawater. *Marine Chemistry* 50, 63–77.
- Moore, J., Doney, S., Lindsay, K., 2004. Upper ocean ecosystem dynamics and iron cycling in a global three-dimensional model. *Global Biogeochemical Cycles* 18, 4.
- Moore, J.K., Braucher, O., 2007. Observations of dissolved iron concentrations in the world ocean: implications and constraints for ocean biogeochemical models. *Biogeosciences Discussions* 4 (2), 1241–1277.
- Moran, S.B., Moore, R.M., 1992. Kinetics of the removal of dissolved aluminum by diatoms in seawater—a comparison with thorium. *Geochimica et Cosmochimica Acta* 56 (9), 3365–3374.
- Morel, F.M., Hudson, R.J., 1985. The geobiological cycle of trace elements in aquatic systems: Redfield revisited. In: Stumm, W. (Ed.), *Chemical Processes in Lakes*. Wiley, pp. 251–281.
- Morel, F.M., Price, N.M., 2003. The biogeochemical cycles of trace metals in the oceans. *Science* 300 (5621), 944–947.
- Murray, J., Barber, R., Bacon, M., Roman, M., Feely, R., 1994. Physical and biological controls on carbon cycling in the equatorial Pacific. *Science* 266 (5182), 58–65.
- Parekh, P., Follows, M., Boyle, E., 2004. Modeling the global ocean iron cycle. *Global Biogeochemical Cycles* 18, 1.
- Parker, A.E., Wilkerson, F.P., Dugdale, R.C., Marchi, A., Hogue, V.E., Landry, M.R., Taylor, A.G., 2011. Spatial patterns of nitrogen uptake and phytoplankton in the equatorial upwelling zone (110–140°W) during 2004 and 2005. *Deep-Sea Research II* 58 (3–4), 417–433.
- Pennington, J.T., Mahoney, K.L., Kuwahara, V.S., Kolber, D.D., Calienes, R., Chavez, F.P., 2006. Primary production in the eastern tropical Pacific: a review. *Progress in Oceanography* 69 (2–4), 285–317.
- Price, N.M., Andersen, L.F., Morel, F.M., 1991. Iron and nitrogen nutrition of equatorial Pacific plankton. *Deep-Sea Research I* 38, 1361–1378.
- Price, N., Ahner, B., Morel, F., 1994. The equatorial Pacific ocean grazer-controlled phytoplankton populations in an iron-limited ecosystem. *Limnology and Oceanography* 39 (3), 520–534.
- Price, N., Morel, F., 1998. Biological cycling of iron in the ocean. *Metal Ions in Biological Systems* 35, 1–36.
- Raimbault, P., Slawyk, G., Boudjellal, B., Coatanoan, C., Conan, P., Coste, B., Garcia, N., Moutin, T., Pujol-Pay, M., 1999. Carbon and nitrogen uptake and export in the equatorial Pacific at 150°W: evidence of an efficient regenerated production cycle. *Journal of Geophysical Research—Oceans* 104 (C2), 3341–3356.
- Resing, J.A., Measures, C.I., 1994. Fluorometric determination of Al in seawater by flow-injection analysis with in-line preconcentration. *Analytical Chemistry* 66 (22), 4105–4111.
- Rodier, M., Le Borgne, R., 1997. Export flux of particles at the equator in the western and central Pacific Ocean. *Deep-Sea Research II* 44 (9–10), 2085–2113.
- Rue, E.L., Bruland, K.W., 1995. Complexation of iron(III) by natural organic ligands in the central north Pacific as determined by a new competitive ligand equilibration adsorptive cathodic stripping voltammetric method. *Marine Chemistry* 50 (1–4), 117–138.
- Rue, E.L., Smith, G.J., Cutter, G.A., Bruland, K.W., 1997. The response of trace element redox couples to suboxic conditions in the water column. *Deep-Sea Research I* 44 (1), 113–134.
- Ryan, J.P., Ueki, I., Chao, Y., Zhang, H., Polito, P.S., Chavez, F.P., 2006. Western Pacific modulation of large phytoplankton blooms in the central and eastern equatorial Pacific. *Journal of Geophysical Research—Biogeosciences* 111 (G2).
- Sarmiento, J.L., Orr, J.C., 1991. 3-dimensional simulations of the impact of Southern Ocean nutrient depletion on atmospheric CO₂ and ocean chemistry. *Limnology and Oceanography* 36 (8), 1928–1950.
- Selph, K.E., Landry, M.R., Taylor, A., Yang, E.J., Measures, C.I., Yang, J.J., Stukel, M.R., Christensen, S., Bidigare, R.R., 2011. Spatially-resolved, taxon-specific phytoplankton production and grazing dynamics in relation to iron distributions in the Equatorial Pacific between 110 and 140°W. *Deep-Sea Research II* 58 (3–4), 358–377.
- Slemmons, L., Gorgues, T., Aumont, O., Menkes, C., Murray, J.W., 2009. Biogeochemical impact of a model western iron source in the Pacific Equatorial Undercurrent. *Deep-Sea Research I* 56, 2115–2128.
- Stewart, R., 2007. *Introduction to Physical Oceanography*. Texas A&M University (on-line textbook).
- Stoffyn, M., 1979. Biological control of dissolved aluminum in seawater—experimental evidence. *Science* 203 (4381), 651–653.
- Strutton, P.G., Ryan, J.P., Chavez, F.P., 2001. Enhanced chlorophyll associated with tropical instability waves in the equatorial Pacific. *Geophysical Research Letters* 28, 2005–2008.
- Strutton, P.G., Palacz, A.P., Dugdale, R.C., Chai, F., Marchi, A., Parker, A.E., Hogue, V., Wilkerson, F.P., 2011. The impact of equatorial Pacific tropical instability waves on hydrography and nutrients: 2004–2005. *Deep-Sea Research II* 58 (3–4), 284–295.
- Takahashi, T., Sutherland, S., Feely, R., Cosca, C., 2003. Decadal variation of the surface water pCO₂ in the western and central equatorial Pacific. *Science* 302 (5646), 852–856.
- Tortell, P., Maldonado, M., Price, N., 1996. The role of heterotrophic bacteria in iron-limited ocean ecosystems. *Nature* 383 (6598), 330–332.
- Tortell, P., Maldonado, M., Granger, J., Price, N., 1999. Marine bacteria and biogeochemical cycling of iron in the oceans. *FEMS Microbiology Ecology* 29 (1), 1–11.
- Tsuchiya, M., 1975. Subsurface countercurrents in eastern equatorial Pacific Ocean. *Journal of Marine Research* 33 (Suppl. S), 145–175.
- Twining, B., Baines, S., Fisher, N., 2004. Element stoichiometries of individual plankton cells collected during the Southern Ocean Iron Experiment (SOFEX). *Limnology and Oceanography* 49 (6), 2115–2128.
- Twining, B.S., Baines, S.B., Bozard, J.B., Vogt, S., Walker, E.A., Nelson, D.M., 2011. Metal quotas of plankton in the equatorial Pacific Ocean. *Deep-Sea Research II* 58 (3–4), 325–341.

- Wang, X., Christian, J., Murtugudde, R., Busalacchi, A., 2006. Spatial and temporal variability in new production in the equatorial Pacific during 1980–2003: physical and biogeochemical controls. *Deep-Sea Research II* 53, 677–697.
- Wells, M.L., Price, N.M., Bruland, K.W., 1995. Iron chemistry in seawater and its relationship to phytoplankton—a workshop report. *Marine Chemistry* 48 (2), 157–182.
- Wells, M.L., Vallis, G.K., Silver, E.A., 1999. Tectonic processes in Papua New Guinea and past productivity in the eastern equatorial Pacific Ocean. *Nature* 398 (6728), 601–604.
- Wu, J., Boyle, E., Sunda, W., Wen, L.-S., 2001. Soluble and colloidal iron in the oligotrophic North Atlantic and North Pacific. *Science* 293, 847–849.
- Wu, J., Boyle, E., 2002. Iron in the Sargasso Sea: implications for the processes controlling dissolved Fe distribution in the ocean. *Global Biogeochemical Cycles* 16, 4.
- Wyrtki, K., 1981. An estimate of the equatorial upwelling in the Pacific. *Journal of Physical Oceanography*, 1205–1214.
- Xiu, P., Chai, F., Shi, L., Xue, H., Chao, Y., 2010. A census of eddy activities in the South China Sea during 1993–2007. *Journal of Geophysical Research* 115, C03012.